ARTICLE

Disruption of *ROBO2* Is Associated with Urinary Tract Anomalies and Confers Risk of Vesicoureteral Reflux

Weining Lu, Albertien M. van Eerde, Xueping Fan, Fabiola Quintero-Rivera,* Shashikant Kulkarni, Heather Ferguson, Hyung-Goo Kim, Yanli Fan, Qiongchao Xi, Qing-gang Li, Damien Sanlaville, William Andrews, Vasi Sundaresan, Weimin Bi, Jiong Yan, Jacques C. Giltay, Cisca Wijmenga, Tom P. V. M. de Jong, Sally A. Feather, Adrian S. Woolf, Yi Rao, James R. Lupski, Michael R. Eccles, Bradley J. Quade, James F. Gusella, Cynthia C. Morton,† and Richard L. Maas

Congenital anomalies of the kidney and urinary tract (CAKUT) include vesicoureteral reflux (VUR). VUR is a complex, genetically heterogeneous developmental disorder characterized by the retrograde flow of urine from the bladder into the ureter and is associated with reflux nephropathy, the cause of 15% of end-stage renal disease in children and young adults. We investigated a man with a de novo translocation, 46,X,t(Y;3)(p11;p12)dn, who exhibits multiple congenital abnormalities, including severe bilateral VUR with ureterovesical junction defects. This translocation disrupts *ROBO2,* which encodes a transmembrane receptor for SLIT ligand, and produces dominant-negative ROBO2 proteins that abrogate SLIT-ROBO signaling in vitro. In addition, we identified two novel *ROBO2* intracellular missense variants that segregate with CAKUT and VUR in two unrelated families. Adult heterozygous and mosaic mutant mice with reduced *Robo2* gene dosage also exhibit striking CAKUT-VUR phenotypes. Collectively, these results implicate the SLIT-ROBO signaling pathway in the pathogenesis of a subset of human VUR.

Congenital anomalies of the kidney and urinary tract (CAKUT) make up a family of diseases with a diverse anatomical spectrum, including kidney anomalies (e.g., renal dysplasia, duplex kidney, and hydronephrosis) and ureter anomalies (e.g., vesicoureteral reflux [VUR], megaureter, and ureterovesical junction [UVJ] obstruction).[1,2] In particular, VUR (MIM %193000), a polygenic genetic disorder with an incidence of ~1 in 100 infants,[3,4] is one of the most common clinical manifestations of CAKUT. VUR is characterized by the reflux of urine from the bladder into the ureters and sometimes into the kidneys and is a risk factor for urinary tract infection (UTI).[5] In combination with intrarenal reflux, the resulting inflammatory reaction may result in renal injury or scarring, also called "reflux nephropathy."[6] Extensive renal scarring impairs renal function and may predispose patients to hypertension, proteinuria, and renal insufficiency. Reflux nephropathy accounts for as much as 15% of end-stage renal disease in children and young adults.[7] Primary VUR results from a developmental defect of the UVJ[8] and is known to occur in multiple members of families. In siblings and offspring of affected patients, the prevalence is as high as 50%.[9,10] Despite its high incidence in the pediatric population, the genetic basis of VUR remains to be elucidated.

Human *ROBO1–4* encode homologs of *Drosophila* Roundabout (Robo), a transmembrane receptor that binds SLIT ligand and transduces a signal to prevent axons from recrossing the CNS midline.[11] On the basis of the mouse *Robo1* mutant phenotype, *ROBO1* is a candidate gene for pulmonary hypoplasia and adenocarcinoma,[12,13] as well as for dyslexia (*DYX5*).[14] Mutations in *ROBO3* result in horizontal-gaze palsy with progressive scoliosis,[15] whereas zebrafish *Robo4* is implicated in angiogenesis.[16] *Robo2* loss-of-function mutations in zebrafish and mice result in retinal and commissural pathfinding defects, respectively.[17,18] Interestingly, *Robo2* and *Slit2* mouse mutants reveal an additional key role for SLIT-ROBO signaling in regulating the metanephric expression of glial cell derived neurotrophic factor (Gdnf), which in turn induces ureteric bud outgrowth from the nephric duct and restricts it to a single site.[19] However, a role for *ROBO2* in human disease has not been identified elsewhere.

From the Genetics Division (W.L.; Y.F.; Q.X.; R.L.M.) and Departments of Pathology (S.K.; B.J.Q.; C.C.M.) and Obstetrics, Gynecology and Reproductive Biology (H.F.; C.C.M.), Brigham and Women's Hospital and Harvard Medical School, Center for Human Genetic Research, Massachusetts General Hospital and Harvard Medical School (F.Q.-R.; H.-G.K.; J.F.G.), and Renal Section, Boston University Medical Center (W.L.; Q.-g.L.), Boston; Departments of Medical Genetics and Pediatric Urology, University Medical Center Utrecht, Utrecht, The Netherlands (A.M.v.E.; J.C.G.; C.W.; T.P.V.M.d.J.); Northwestern University Institute of Neuroscience, Chicago (X.F.; Y.R.); Genetics Department, Hôpital Necker-Enfants Malades, Paris (D.S.); Medical Research Council Centre for Developmental Neurobiology, King's College of London (W.A.; V.S.), and Nephro-Urology Unit, Institute of Child Health, University College London (A.S.W.), London; Department of Molecular and Human Genetics, Baylor College of Medicine, Houston (W.B.; J.Y.; J.R.L.); Department of Pediatric Nephrology, St. James' University Hospital, Leeds, United Kingdom (S.A.F.); and Pathology Department, University of Otago, Dunedin, New Zealand (M.R.E)

Received November 9, 2006; accepted for publication January 15, 2007; electronically published February 14, 2007.

Address for correspondence and reprints: Dr. Richard Maas, Genetics Division, NRB 458, Brigham and Women's Hospital, Harvard Medical School, 77 Avenue Louis Pasteur, Boston, MA 02115. E-mail: maas@genetics.med.harvard.edu

* Present affiliation: Department of Pathology, The David Geffen School of Medicine at University of California–Los Angeles, Los Angeles.

† All editorial responsibility for this article was handled by an associate editor of the *Journal*.

Am. J. Hum. Genet. 2007;80:616–632. 0002-9297/2007/8004-0005$15.00
DOI: 10.1086/512735

Material and Methods

FISH and Array Comparative Genomic Hybridization Analyses

Metaphase FISH was performed according to standard methods. RP11 BAC clones were obtained from BACPAC Resources, were labeled as FISH probes, and were hybridized to metaphase chromosomes prepared from a t(Y;3)(p11;p12)dn lymphoblastoid cell line established from patient DGAP107. Array comparative genomic hybridization (CGH) experiments were performed by Spectral Genomics (SpectralChip 2006 array) and Agilent Technologies (Human Genome CGH Microarray Kit 44A).

Southern and RT-PCR Analyses

Southern and RT-PCR analyses were performed according to routine protocols. RT-PCR primers used to amplify the 2.8-kb *ROBO2* cDNA (GenBank accession number NM_002942) were *ROBO2-F1* and *ROBO2-R1*; those used to amplify ROBO2-PCDH11Y fusion transcripts were *ROBO2-F2* (same for all transcripts) and *PCDH11Y-R1, PCDH11Y-R2,* and *PCDH11Y-R3*; those used to amplify wild-type *ROBO2* transcripts were *ROBO2-F2* and *ROBO2-qR*; and those used to amplify *PCDH11Y* cDNA (GenBank accession number NM_032971) were *PCDH11Y-rtF1* and *PCDH11Y-rtR1* (appendix C). All primer sequences are listed in appendix G.

Quantitative Real-Time PCR Analyses

PCR primers and TaqMan fluorogenic probes for analysis of the *ROBO2* nontranslocated allele and the *Fu-129* and *Fu-153* fusion transcripts were designed using Primer Express software (Applied Biosystems). TaqMan primers and probes for *Gapdh* and *β-actin* were used for normalization. Probe melting temperatures were ~7°C–10°C higher than those for the matching primer pair. High-pressure liquid chromatography–purified fluorogenic probes contained covalently attached 5′-FAM reporter and 3′-BHQ1 quencher dyes. Sequences of TaqMan primer and probe sets are listed in appendix G. RT-PCR reactions were performed using an iCycler IQ Real-Time Detection System (Bio-Rad). SuperScript One-Step RT-PCR with Platinum Taq kits (Invitrogen) were used for triplicate RT-PCR amplifications, with each 50-μl reaction containing 200 ng total RNA, 5 mM $MgSO_4$, 500 nM forward and reverse primers, and 200 nM fluorogenic probes. Controls included either no reverse transcriptase or the substitution of H_2O for RNA for each primer and probe set. The one-step RT-PCR protocol was 15 min at 50°C and 5 min at 95°C, followed by 45 cycles, each consisting of 15 s at 95°C and 1 min at 60°C. IQ Supermix reagent for real-time PCR (Bio-Rad) was used for two-step RT-PCR. Relative gene expression was analyzed using standard curve and comparative threshold cycle methods.

Fusion Proteins

cDNA sequences for Fu-129 and Fu-153 were amplified by PCR with the use of forward primer 5′-hR2(E1) and reverse primers 3′-LEVA(X1) and 3′-SRSC(X1) (appendix G) cloned into *Eco*RI and *Xho*I sites in pcDNA3, under control of the cytomegalovirus promoter. To express yellow fluorescent protein (YFP)–ROBO2-PCDH11Y fusions, the YFP (Venus) coding sequence was cloned into *Bam*HI and *Eco*RI sites in pCS, whereas *ROBO2-PCDH11Y* coding sequences were inserted inframe with YFP at *Eco*RI and *Xho*I sites. YFP-ROBO2-PCDH11Y fusion proteins were expressed under the control of the simian cytomegalovirus IE94 promoter. Myc-SLIT and hemagglutinin (HA)–RoboN (Robo1-N) constructs have been described elsewhere.[20]

Neuronal Migration Assay

The in vitro neuronal migration assay that uses postnatal anterior subventricular zone (SVZa) cells was described elsewhere.[21] In brief, P1-6 Sprague-Dawley rat brains devoid of meninges were placed in 10% fetal calf serum in Dulbecco's modified Eagle medium (DMEM) and were embedded. Coronal sections of 300 μm were prepared by vibratome, and tissues within the SVZa borders were dissected to make SVZa explants 200–300 μm in diameter. Explants were embedded, together with human embryonic kidney (HEK) cell aggregates in collagen and matrigel (3:2:1 ratio of collagen:matrigel:medium), and were cultured in DMEM with 5% CO_2 at 37°C for 24 h. Cocultured cells were washed in PBS for 10 min and were fixed in 4% paraformaldehyde at 4°C overnight.

To make cell aggregates, HEK cells were transiently transfected to express mouse Slit2 or RoboN, DGAP107 Fu-129 or Fu-153, or pcDNA3 or Semaphorin 3A expression vectors as negative controls, with the use of Effectene Transfection Kit (Qiagen). After 24 h, transfected HEK cells were detached and were collected by brief centrifugation, and cell pellets were resuspended in an equal volume of DMEM. Ten microliters of suspended cells were hung from the dish cover at 37°C, in 5% CO_2 for 1–2 h, to form aggregates. Aggregated cells were washed in DMEM and were squared with a needle.

Western Blot

HEK cells were transfected to express YFP-ROBO2-PCDH11Y-Fu-129, YFP-ROBO2-PCDH11Y-Fu-153, Myc-Slit, and HA-RoboN. Cells transfected with pCS2 vector were used as a negative control. To remove cell debris 48 h after transfection, media were collected and were centrifuged for 20 min at 4°C. Supernatants were diluted with sixfold protein loading buffer and were heated at 95°C for 20 min. Cells were lysed (1 × PBS, 0.5% Triton X-100, and 1 × protease inhibitor), were diluted with sixfold protein loading buffer, and were heated at 95°C for 20 min. Proteins were resolved by 12% SDS-PAGE, with YFP (Venus) fusion proteins detected by monoclonal anti–green fluorescent protein (GFP) antibody that detects YFP (Clontech), and Myc-Slit2 and HA-RoboN were blotted with monoclonal antibodies against Myc and HA, respectively.

Mutation Analysis

ROBO2 mutation screening employed PCR amplification of each of the 26 human *ROBO2* exons and intron-exon boundaries, followed by purification and bidirectional DNA sequencing. Sequences of the *ROBO2* PCR primer sets are listed in appendix G. Sequence data were analyzed using Lasergene (DNAStar) sequence analysis software. DNA samples with sequence changes were confirmed by resequencing. National Center for Biotechnology Information RefSeq *ROBO2* cDNA sequence (GenInfo identifier [GI] 109254774) and protein sequence (Entrez Protein accession number NP_002933) (GI 61888896) were used to calculate the nucleotide and amino acid positions.

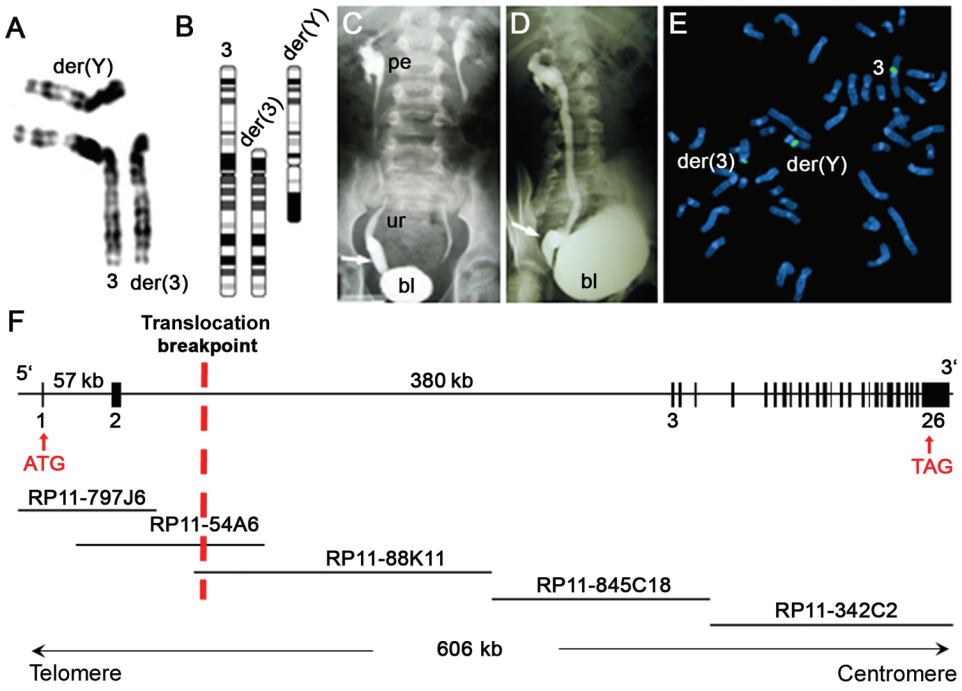

Figure 1. *ROBO2* disrupted in DGAP107. Partial karyogram (*A*) and idiogram (*B*) for 46,X,t(Y;3)(p11;p12)dn is shown. VCUG of DGAP107 shows anterior-posterior (*C*) and lateral (*D*) views of bilateral grade IV VUR and megaureter at the right UVJ (*arrows*). bl = Bladder; pe = renal pelvis; ur = ureter. *E,* FISH analysis showing BAC RP11-54A6 (*green*), which hybridizes to normal chromosome 3, der(3), and der(Y) and crosses the 3p12 breakpoint. *F,* Intron-exon structure of *ROBO2,* with select exons numbered and the relevant BAC contig. The location of the 3p12 translocation breakpoint is indicated by a red dotted vertical line.

Preparation of Robo2^{flox} *and* Robo2^{del5} *Alleles*

Robo2^{flox} mice were produced using homologous recombination in 129 embryotic stem cells and blastocyst injection. After germline transmission, mice were backcrossed to C57BL/6 and were analyzed thereafter in a mixed C57BL/6-129/Sv background. The *Robo2*^{flox} allele was genotyped by PCR amplification, followed by *Spe*I restriction digestion with the use of PCR primers *Ro2-MEBAC15F* and *Ro2-MEBAC15R* (appendix G), which amplify a 1,100-bp fragment for both wild-type and *Robo2*^{flox} alleles. After *Spe*I digestion, the *Robo2*^{flox} amplicon remains uncut, whereas the wild-type amplicon yields 750-bp and 350-bp products. *Robo2*$^{flox/+}$ mice were bred with *Tg*$^{EIIa\text{-}Cre}$ (stock number 003724 [Jackson Laboratory]) to produce the *Robo2*^{del5} allele. The *Robo2*^{del5} allele was amplified by primers *Robo2koF* and *Robo2R,* which produce a 1,100-bp fragment. The wild-type allele was amplified by primers *Robo2wtF* and *Robo2R,* which yield a 1,390-bp fragment. F2 *Robo2*$^{del5/del5}$↔*Robo2*$^{del5/flox}$ mosaic mice were prepared as described in appendix F and were analyzed for the presence of urinary tract phenotypes. To examine the ureter and kidney defects, *Hoxb7-GFP* transgenic mice (gift from Dr. Frank Costantini, Columbia University) were bred with *Robo2* mutants. GFP fluorescence was monitored and photographed using a Nikon SMZ-1500 epifluorescence stereomicroscope.

Human and Animal Studies

All human studies were performed under informed consent protocols approved by the Partners HealthCare System Human Research Committee (Boston), the Human Research Ethics Committee (Institute of Child Health, University College London), or the University Medical Center (Utrecht). Mouse protocols were approved by the Institutional Animal Care and Use Committee at Harvard Medical School or Boston University Medical Center, with additional approval from King's College, London.

Results

The Developmental Genome Anatomy Project (DGAP) is a collaborative effort to use chromosomal rearrangements associated with developmental disorders to identify the underlying genetic etiology. DGAP107 is a man aged 18 years with a 46,X,t(Y;3)(p11;p12)dn translocation, whose phenotype includes bilateral high-grade VUR and right megaureter at the UVJ (fig. 1*A*–1*D* and appendix A). He required ureteral reimplantation surgery at age 9 years and was found to have wide-open right and left ureteral orifices due to bilateral absence of intravesical ureteral segments. Normally, these submucosal ureteral segments obliquely traverse the muscular layers of the bladder to prevent retrograde flow of urine by a flap-valve mechanism. By metaphase FISH, we identified a BAC clone (RP11-54A6) that crosses the 3p12 breakpoint, which disrupts intron 2 of *ROBO2,* which is composed of 26 exons and spans ~606 kb of genomic DNA (fig. 1*E* and 1*F*).

We cloned and sequenced the breakpoints on the der(3) and der(Y) chromosomes (appendix B). In addition to

disruption of *ROBO2* at 3p12, the protocadherin gene *PCDH11Y* at Yp11 was also disrupted by the translocation. A contribution of *PCDH11Y* disruption to the VUR phenotype in DGAP107 is unlikely, however, since *PCDH11Y* expression has been detected only in placenta, brain, retina, and testis[22] and has not been detected in embryonic kidney (appendix C). By array CGH and FISH, we also identified a 3.4-Mb interstitial deletion at 17p11.2 in DGAP107. This region is within the common microdeletion region pathogenetic in Smith-Magenis syndrome (SMS [MIM #182290]), a mental retardation syndrome associated with behavioral and sleep disturbances and craniofacial and skeletal anomalies.[23] Thus, a role for del(17)(p11.2) in the sleep, behavioral, and cognitive deficits of DGAP107 seems likely. The del(17)(p11.2) microdeletion could also contribute to the pathogenesis of VUR in DGAP107. However, for reasons described below and in appendix D, we conclude that *ROBO2* disruption alone is sufficient to account for the VUR phenotype observed in DGAP107.

The t(Y;3) translocation in DGAP107 juxtaposes *ROBO2* and *PCDH11Y* in the same transcriptional orientation. On the der(Y), the promoter and the first two exons of *ROBO2* reside upstream of exons 1d–6 of *PCDH11Y* (fig. 2*A*). From RT-PCR experiments that used DGAP107 lymphoblast RNA, we identified two *ROBO2-PCDH11Y* fusion transcripts driven by the *ROBO2* promoter (fig. 2*B*). Each transcript contains the first two exons of *ROBO2* spliced out of frame to *PCDH11Y* downstream exons, resulting in premature stop codons shortly after *ROBO2* exon 2. When assayed by real-time RT-PCR, these fusion transcripts, denoted Fu-129 and Fu-153, are expressed at somewhat reduced levels compared with the wild-type *ROBO2* transcripts derived from the nontranslocated allele (fig. 2*C*); the wild-type transcripts contained no detectable mutations. Fu-129 and Fu-153 encode 129- and 153-residue polypeptides, respectively, containing the first ROBO2 extracellular immunoglobulin (Ig) domain, but they are truncated before the transmembrane and cytoplasmic domains required for SLIT-ROBO signal transduction (fig. 2*D*).

When expressed without transmembrane and cytoplasmic domains, the soluble extracellular Ig domains of ROBO, denoted as RoboN, are able to bind SLIT ligand.[24] Moreover, the first ROBO Ig domain is necessary and potentially sufficient for SLIT binding.[24] RoboN isoforms can thus inhibit SLIT-ROBO signaling by competing with wild-type ROBO for SLIT binding.[25] We therefore hypothesized that the truncated proteins encoded by the ROBO2-PCDH11Y fusions might act in a dominant-negative manner to block endogenous SLIT-ROBO signaling. To test this hypothesis, we performed an in vitro neuronal migration

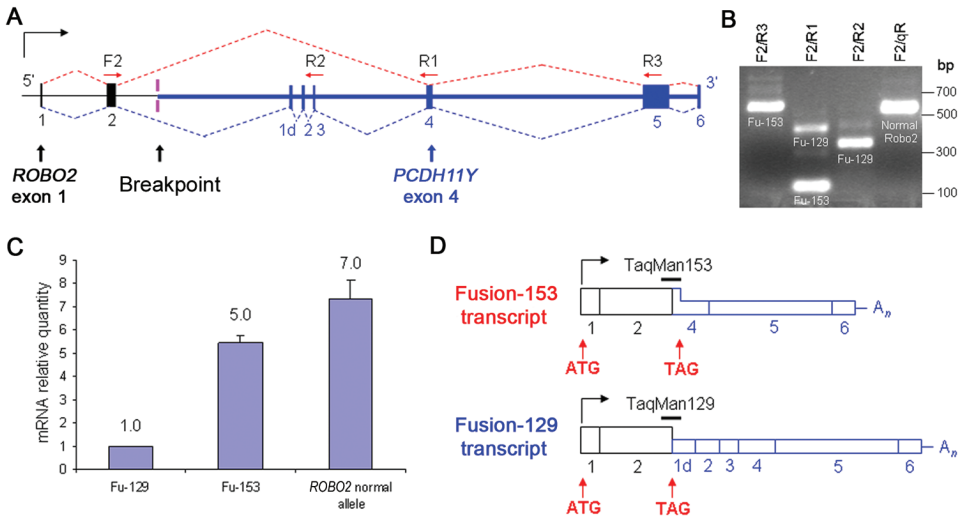

Figure 2. The t(Y;3) translocation in DGAP107, which generates novel *ROBO2* fusion transcripts. *A, ROBO2* and *PCDH11Y* intron-exon structure surrounding the der(Y) breakpoint. The forward primer F2 in *ROBO2* exon 2 (*black bar*) was used in RT-PCR with three reverse primers—R2, R1, and R3—in *PCDH11Y* exons 3, 4, and 5, respectively (*blue bars*). Dotted lines indicate the observed splicing patterns of the two fusion transcripts. The red splicing pattern generates Fu-153, which encodes 153 aa, and the blue pattern generates Fu-129, which encodes 129 aa. *B,* RT-PCR fusion transcript amplification. *Lane 1,* F2/R3 primers amplify Fu-153 (641 bp) and Fu-129 transcripts; only the shorter Fu-153 amplicon is shown. *Lane 2,* F2/R1 primers amplify transcripts for both Fu-129 (456 bp) and Fu-153 (122 bp). *Lane 3,* F2/R2 primers amplify only Fu-129 transcripts (347 bp). *Lane 4,* F2/qR primers amplify only transcripts from the wild-type nontranslocated *ROBO2* allele (606 bp). qR primer is located in exon 7 of *ROBO2*. *C,* Real-time RT-PCR quantitation of *ROBO2* fusion transcripts Fu-129 and Fu-153 (detected by TaqMan probes shown in panel D) and of *ROBO2* nontranslocated allele transcripts (detected by TaqMan probe across *ROBO2* exons 2 and 3) in DGAP107 lymphoblast RNA. *D,* Exon structure of Fu-153 and Fu-129. Horizontal bars indicate TaqMan probes used to quantify fusion transcripts. Black boxes indicate *ROBO2* exons; blue boxes, *PCDH11Y* exons; full-height boxes, coding exons; and half-height boxes, noncoding exons.

assay[21] in which SVZa explants were cultured in proximity to HEK cell aggregates secreting Slit2 or Slit2 and either RoboN, Semaphorin 3A, Fu-129, or Fu-153 (fig. 3*A*). We then examined the directionality of neuronal migration away from the SVZa explants (fig. 3*B*–3*F*). HEK cell aggregates alone have no effect on SVZa explants, resulting in a radially symmetric pattern of neuronal outgrowth.[25]

When they were cultured with HEK cell aggregates transfected with vectors expressing Slit2 only or Slit2 and Semaphorin 3A (a molecule having no effect on Slit function, as a control), the Slit2-expressing cell aggregates acted upon the SVZa explants to repel SVZa neuronal outgrowth (fig. 3*B* and 3*C*). In contrast, in aggregates coexpressing Slit2 and either RoboN, Fu-129, or Fu-153, the latter molecules abrogated the chemorepulsive effect of Slit2 on the SVZa explant and significantly increased the number of neurons able to migrate towards the Slit2 source, resulting in a radially symmetric pattern of neuronal outgrowth (fig. 3*B*–3*F*). These results indicate that the ROBO2-PCDH11Y fusion proteins that result from t(Y;3) can act as dominant-negative molecules to block SLIT-mediated chemorepulsive function. The fusion proteins could further compromise ROBO2 function in DGAP107, which retains only hemizygous *ROBO2* expression from the nontranslocated allele.

Family studies indicate that primary VUR frequently segregates with autosomal dominant inheritance and incomplete penetrance.[9,26] To test whether mutations in *ROBO2* are associated with CAKUT and VUR in the general population, we sequenced the 26 exons and intron-exon boundaries of *ROBO2* in 124 families with VUR with potential autosomal dominant inheritance. One sequence change—c.2436T→C, or I598T—was observed in exon 12 in the ROBO2 extracellular domain but was also identified in three control DNA samples (see below). It therefore most likely represents a sequence polymorphism and was discounted from further study. In contrast, two novel *ROBO2* intracellular coding sequence changes were identified that were not found in 276 controls (see below). These produce nonconservative amino acid substitutions in two independent families with CAKUT-VUR (fig. 4 and appendix E). In family 2559x with CAKUT-VUR, the affected daughter, 25592, has bilateral VUR, hypoplastic kidneys, and nephropathy, whereas her mother, 25593, required ureteral reimplantation because of severe VUR (fig. 4*A*–4*C*). Both individuals have a heterozygous T→C change at position 3477 in coding exon 19 (c.3477T→C) that would cause a nonconservative missense I945T substitution in the ROBO2 intracellular domain (ICD) (fig. 4*D* and 4*E*).

In family B5 with CAKUT-VUR, the proband has bilateral VUR and a right duplex collecting system and kidney. Her mother and two aunts have urinary tract symptoms and ultrasonographical evidence of CAKUT, whereas her grandmother has a unilateral small kidney (fig. 4*F*–4*I*). All five family members carry a heterozygous G→A sequence alteration at position 4349 in coding exon 23 (c.4349G→A) that would cause a nonconservative missense amino acid

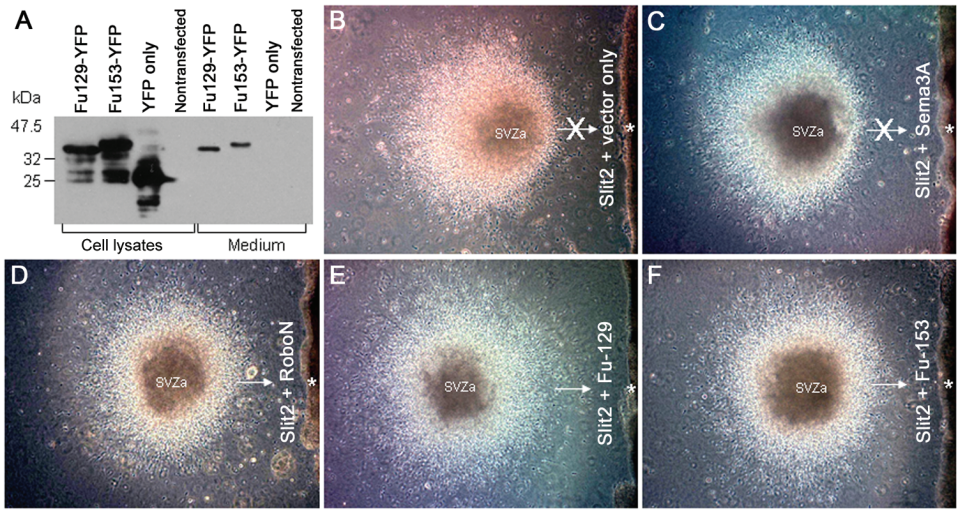

Figure 3. ROBO2 fusion proteins inhibiting SLIT chemorepulsion. *A,* YFP-tagged ROBO2 fusion proteins (Fu129-YFP [40 kDa] and Fu153-YFP [42 kDa]) detected by an anti-YFP antibody, expressed in HEK cell lysates, and secreted into the medium. In the presence of aggregated cells transfected with Slit2 plus empty vector (*B*) or Slit2 plus Sema3A (Semaphorin 3A, with no effect on Slit2 repulsive activity) (*C*), cells migrate out of SVZa explants and away from the Slit2-expressing cell aggregate (*asterisk*). In the presence of aggregated cells transfected with Slit2 plus RoboN (the Robo extracellular domain, which inhibits Slit repulsive activity), cells migrate out of SVZa explants symmetrically in all directions (*D*) including toward (*arrow*) the Slit2 and RoboN-expressing cell aggregate (*asterisk*). Fu-129 and Fu-153 also effectively block Slit2 repulsive activity (*E* and *F*), allowing symmetrical neuronal migration out of SVZa explants and toward (*arrows*) Slit2 and Fu-129 or Slit2– and Fu-153–expressing cell aggregates (*asterisks*).

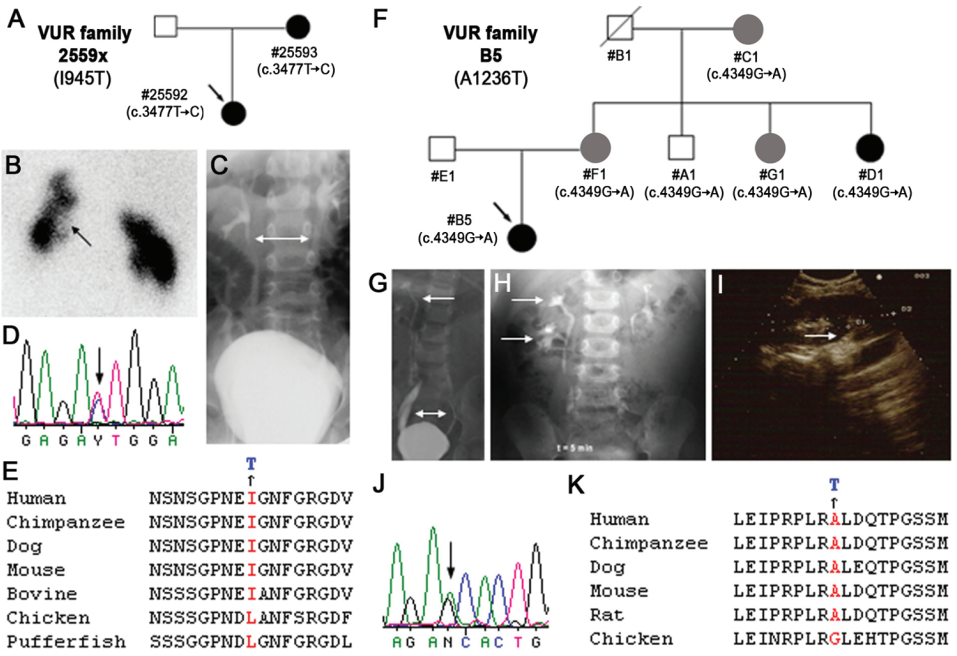

Figure 4. *ROBO2* missense mutations in familial CAKUT and VUR. *A,* Family 2559x with CAKUT-VUR and exon 19 (c.3477T→C) mutation. Arrow indicates the proband. Blackened and gray symbols indicate patients with CAKUT-VUR and family members with urinary tract symptoms and radiological evidence of CAKUT. Nucleotide changes are shown under each individual. *B,* 99mTc-dimercaptosuccinic acid renogram of proband 25592 showing bilateral renal parenchymal defects (*arrow*). *C,* VCUG of proband 25592 showing bilateral reflux (*bidirectional arrow*). Chromatograms show T→C change (*arrow*) in exon 19 of family 2559x (*D*) and amino acid conservation across species (*E*). *F,* Family B5 with CAKUT-VUR and exon 23 (c.4349G→A) mutation. *G,* VCUG showing bilateral VUR (*bidirectional arrow*) and right duplex kidney (*arrow*) in proband B5. *H,* IVP detecting right duplex kidney (*arrows*) in proband B5. *I,* US showing suspected duplex (*arrow*) in upper pole of the right kidney in D1, an asymptomatic aunt of proband B5. Chromatograms show G→A change (*arrow*) in exon 23 of family B5 (*J*) and amino acid conservation across species (*K*).

substitution, A1236T, in the ROBO2 ICD (fig. 4*J* and 4*K*). An additional family member, uncle A1, also has this alteration but did not exhibit an ultrasonographically detectable renal phenotype; however, nonpenetrance of VUR is common.[9] Both I945 and A1236 are evolutionarily conserved in all mammals and are only slightly divergent in birds and fish, organisms that lack a urinary bladder and UVJ (fig. 4*E* and 4*K*).

To further assess the likelihood that these sequence changes represent functional missense variants, as opposed to rare neutral variants found in the general population, we sequenced *ROBO2* exons 12, 19, and 23 in 180 unrelated, clinically unaffected controls of ethnic backgrounds similar to those of the affected individuals. Two occurrences of c.2436T→C in exon 12 were detected, but no nucleotide changes were identified in exons 19 or 23. In addition, to determine the full spectrum of *ROBO2* sequence variation, we resequenced the 26 *ROBO2* exons and intron-exon boundaries in an additional 96 controls. We found only one reoccurrence of c.2436T→C. Of several nonvalidated putative synonymous and nonsynonymous *ROBO2* coding SNPs listed in Ensembl v39, we detected only one—c.737C→A, or R32R—in our own sequencing efforts. Moreover, this apparent change was found to represent a sequencing artifact. Thus, in sum, these results suggest that the two sequence changes in the ICD identified in familial VUR are deleterious missense variants that contribute to the CAKUT-VUR phenotype.

Both I945T and A1236T could alter the function of the ROBO ICD, which regulates actin polymerization and cellular migration,[27] by creating novel threonine phosphorylation sites or by influencing the binding of proteins that interact with the ROBO ICD.[28] For example, the SH3 domain of srGAP1 binds to the ROBO1 ICD CC3 subdomain,[27,28] which is partly conserved in ROBO2. The ROBO2 CC3 subdomain (residues 1193–1201) resides close to A1236, and an extended ROBO1 CC3 peptide binds the srGAP1 SH3 domain much more strongly than does the isolated CC3,[27] suggesting that residues outside CC3 also mediate srGAP binding. I945T and A1236T may act as either dominant gain- or loss-of-function mutations that influence protein binding to the ROBO2 ICD.

To establish further the involvement of *ROBO2* in the pathogenesis of the CAKUT-VUR phenotype postnatally, we next generated and analyzed a conditional *Robo2* mouse mutant. A homozygous *Robo2*-null mouse, described elsewhere,[19] with a targeted deletion of exon 1 exhibits a multiple ureter phenotype and fails to survive

after birth. To determine whether heterozygosity for *Robo2* loss of function could produce an abnormal urinary tract phenotype and recapitulate human CAKUT-VUR, we prepared a mouse *Robo2* floxed allele, *Robo2*^{flox}, containing *loxP* sites flanking *Robo2* exon 5 (fig. 5*A*). *Robo2*$^{flox/flox}$ homozygotes are viable and fertile and lack urinary tract abnormalities. We then produced *Robo2*$^{del5/+}$ mice that lack exon 5, by crossing the floxed allele with the *Tg*$^{EIIa\text{-}Cre}$ deletor strain.[29] The deletion of *Robo2* exon 5 causes a reading frameshift. RT-PCR and in situ hybridization experiments showed that *Robo2*^{del5} transcripts were expressed at markedly reduced levels compared with transcripts from the wild-type allele. We thus conclude that *Robo2*^{del5} is, effectively, a null allele. Consistent with results reported for the *Robo2* null allele described elsewhere,[19] *Robo2*$^{del5/del5}$ homozygotes uniformly died shortly after birth with multiplex, dysplastic kidneys and short ureters (fig. 5*B*–5*E*). However, whereas no heterozygous phenotype was described for the existing *Robo2* null allele,[19] when a *Hoxb7-GFP* reporter transgene that specifically identifies the ureteric epithelium[30] was introduced into the *Robo2*$^{del5/+}$ background, 4 (15%) of 26 *Robo2*$^{del5/+}$ heterozygous newborns exhibited a unilateral CAKUT-VUR phenotype (fig. 5*F* and fig. 5*G*). This heterozygous phenotype included both massive and lesser degrees of megaureter and a wide-open UVJ, similar to the pathology identified in DGAP107.

To test whether further reductions in *Robo2* gene dosage could increase CAKUT-VUR penetrance, we took advan-

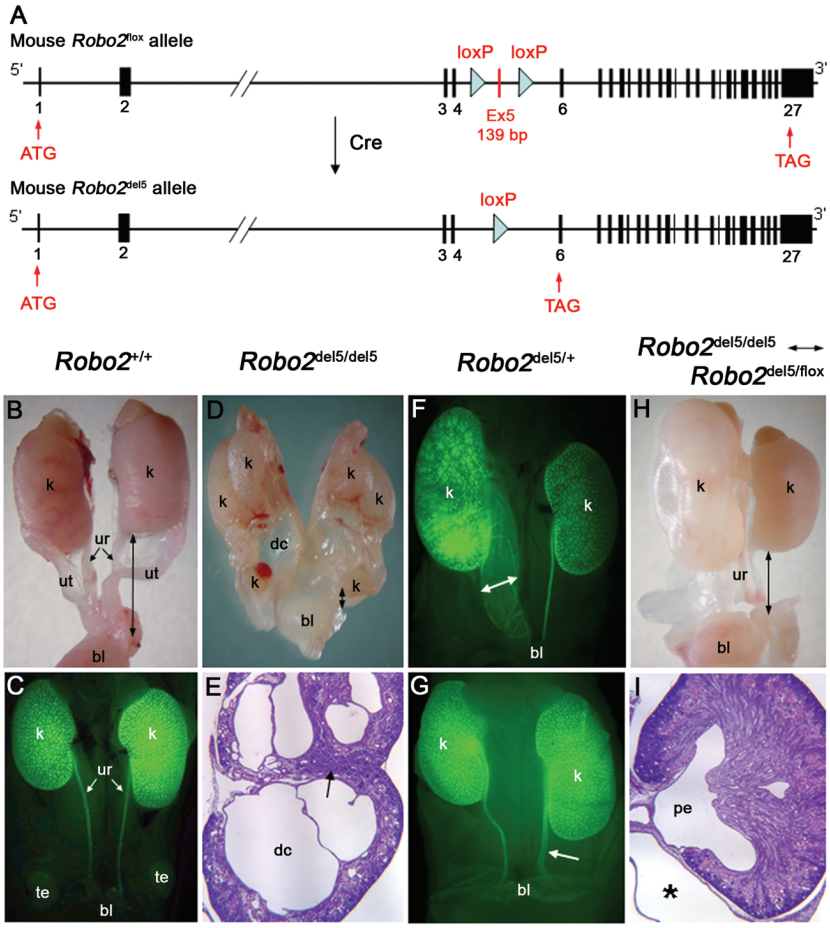

Figure 5. *Robo2*$^{del5/del5}$ homozygous, *Robo2*$^{del5/+}$ heterozygous, and *Robo2*$^{del5/del5}$↔*Robo2*$^{del5/flox}$ mosaic newborn mice expressing striking CAKUT phenotypes. *A,* Structures of the mouse *Robo2*^{flox} and *Robo2*^{del5} alleles. The *Robo2*^{flox} allele encodes a wild-type, full-length 1,470-aa Robo2 protein but contains two *loxP* sites flanking exon 5. The *Robo2*^{del5} allele is generated from *Robo2*^{flox} by Cre, which deletes *Robo2* exon 5 to produce an aberrant transcript expressed only at low levels. *B* and *C,* Wild-type female (*B*) and male (*C*) newborn mouse excretory system. The male excretory system in panel C is illuminated by the *Hoxb7-GFP* transgene. k = kidney; bl = bladder; ur = ureter; ut = uterus; te = testis. Black bidirectional arrows indicate ureter length in panels B and D. *Robo2*$^{del5/del5}$ newborn homozygotes display multiplex dysplastic kidneys (*D*) and, at 25× magnification (*E*), reveal dysplastic cysts (dc) in the calyces and an internalized nephrogenic zone (*arrow*). *Hoxb7-GFP* transgene–positive *Robo2*$^{del5/+}$ heterozygous newborns show megaureter dilation (*F*) (*bidirectional arrow*) and early ureter dilatation (*G*) (*arrow*). *Robo2*$^{del5/del5}$↔*Robo2*$^{del5/flox}$ mosaic newborns show hydronephrosis in the left kidney (*H*). At 25× magnification (*I*), they show megaureter (*asterisk*). Black bidirectional arrows indicate ureter length in panel H. pe = pelvis.

tage of the variable expression of the *EIIa*-directed Cre recombinase in the early preimplantation embryo,[31] to generate mosaic progeny that consisted of admixtures of *Robo2*$^{del5/del5}$ (null) and *Robo2*$^{del5/flox}$ (haploinsufficient) cells. This mosaicism originates from the incomplete, stochastic action of the *EIIa-Cre* transgene on the *Robo2*^{flox} allele in the early embryo before implantation.[31] Remarkably, 4 (40%) of 10 *Robo2*$^{del5/del5}$↔*Robo2*$^{del5/flox}$ mosaic newborns (resulting from the union of *Robo2*^{del5};*Tg*$^{EIIa\text{-}Cre}$ and *Robo2*^{flox} gametes) exhibited unilateral urinary tract defects, including short ureter, megaureter, and hydronephrosis (fig. 5*H* and 5*I*).

To determine whether *Robo2*$^{del5/del5}$↔*Robo2*$^{del5/flox}$ mosaic newborns with urinary tract defects could survive after prolonged reflux and obstruction, we followed another cohort of these mice to adulthood. Seven (70%) of 10 *Robo2*$^{del5/del5}$↔*Robo2*$^{del5/flox}$ adult mosaics, ranging in age from 45 d to 77 d, manifested defects involving the UVJ (fig. 6). These UVJ defects were bilateral and especially notable, in that one UVJ was typically located laterally and cephalad in the bladder (fig. 6*A*–6*D*), a location commonly associated with reflux in humans,[32] whereas the contralateral UVJ was located caudad in the bladder or even ectopically in the urethra. The caudal UVJ location was associated with obstruction, resulting in megaureter and severe hydronephrosis (fig. 6*C* and 6*E*). In some male *Robo2*$^{del5/del5}$↔*Robo2*$^{del5/flox}$ mice, the ureter was connected to the vas deferens, resulting in massive hydronephrosis (fig. 6*F*). The *Robo2*$^{del5/del5}$↔*Robo2*$^{del5/flox}$ mouse model is thus consistent with the frequent coexistence of reflux and obstruction in the same patient with VUR.[33] During embryonic development, the nephric duct undergoes apoptosis, transposing the ureter orifice from the nephric duct to the urogenital sinus epithelium, to form the UVJ.[34] Mutation in mouse *Robo2* causes abnormal sites of ureteric bud outgrowth,[19] which provides a developmental explanation for the ectopic UVJ sites frequently observed in VUR.

Discussion

Collectively, these results demonstrate that reduced *Robo2* gene dosage can contribute to the pathogenesis of CAKUT-VUR (table 1 and appendix F). In human primary VUR,

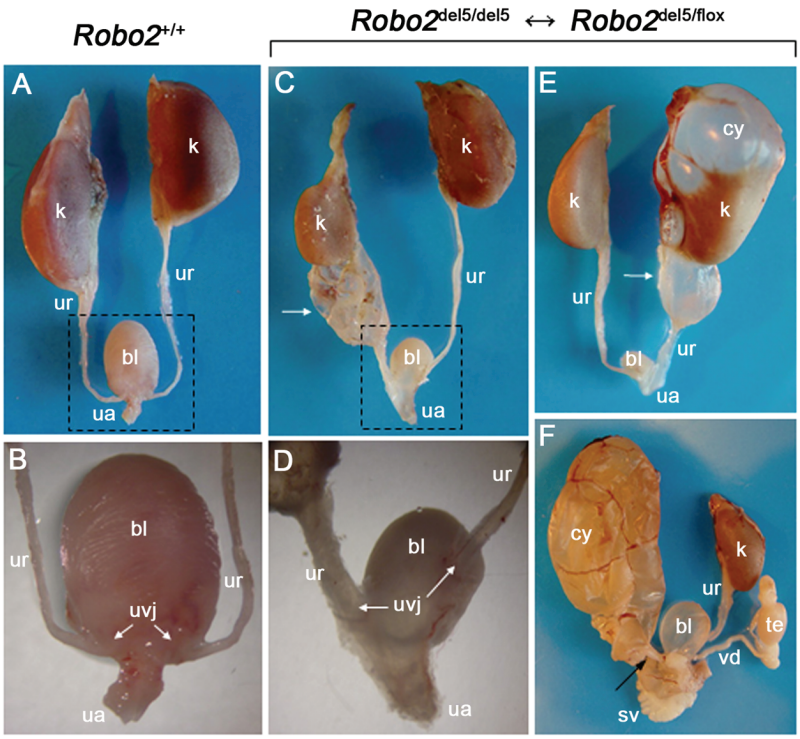

Figure 6. Adult *Robo2*$^{del5/del5}$↔*Robo2*$^{del5/flox}$ mosaics exhibiting megaureter, hydronephrosis, and UVJ defects. *A–D,* Ventral views. k = kidney; ur = ureter; bl = bladder; ua = urethra. *A,* Urinary tract in a wild-type mouse aged 87 d. *B,* Higher magnification of boxed region in panel A, indicating normal position of the UVJ. *C,* Right megaureter (*arrow*) in a *Robo2*$^{del5/del5}$↔*Robo2*$^{del5/flox}$ mosaic aged 45 d. *D,* Higher magnification of boxed region in panel C, demonstrating abnormal bilateral UVJ. The obstructed right UVJ connects to a caudal site in the bladder close to the urethra, causing megaureter. The left UVJ is located laterally in the bladder, a site commonly associated with human VUR. *E* and *F,* Dorsal views. *E,* Right megaureter (*arrow*) and hydronephrosis in a mosaic aged 45 d. Hydronephrosis replaces the normal renal parenchyma (k), causing an upper pole cyst (cy). *F,* Left ureter of a male mosaic mouse aged 77 d that remains connected to the vas deferens (vd) (*arrow*), resulting in obstruction and severe hydronephrosis. The left kidney has lost all parenchyma and is replaced by a large cyst. The right kidney, ureter, and vas deferens are normal in appearance. sv = seminal vesicle; te = testis.

Table 1. Penetrance of CAKUT in *Robo2*^{del5} Mutant Mice

Genotype	*Robo2*$^{del5/+}$ Newborn	*Robo2*$^{del5/flox}$ Mosaic Newborn	*Robo2*$^{del5/flox}$ Mosaic Adult	*Robo2*$^{del5/del5}$ Newborn
CAKUT penetrance (%)	15	40	70	100
Total number observed	26	10	10	20

linkage studies have produced inconsistent results,[35] underscoring the need for other methods to identify the responsible genes. This problem is especially acute for VUR, since the manifestations may vary during life, progressing or resolving spontaneously.[36] Furthermore, because asymptomatic individuals cannot be classified as "unaffected," linkage studies may be inconclusive or yield false-negative results unless confined to affected individuals.[36]

Lastly, intrafamilial phenotypic variability and genetic heterogeneity[3,35] also exist. Since we identified only two coding-region changes segregating with VUR in 124 families with VUR, alterations in *ROBO2* itself are likely to account for a small subset of VUR. Interestingly, however, recent studies indicate that *ROBO2* resides in an inherently unstable genomic region, 3p12.3, that is prone to evolutionary chromosomal rearrangements and to loss of heterozygosity in human cancers.[37] This raises the yet-untested possibility that *ROBO2* may be subject to frequent rearrangement or microdeletion and duplication at either the organismal or cellular level, which could be missed by direct sequencing. In addition, variants in other genes whose products function in the ROBO2 signal-transduction pathway may be implicated in the molecular pathogenesis of renal dysplasia and VUR, which may coexist because of interrelated pathophysiology, common underlying genetic abnormality, or both mechanisms.

Acknowledgments

We thank Roxana Peters, Robert Eisenman, Diana Donovan, Annick Turbe-Doan, and Juan Liu, for technical support; Yiping Shen, Anne Higgins, and Fowzan Alkuraya, for assistance with array CGH; Chantal Farra, for referral of the DGAP107 subject; Frank Costantini, for providing *Hoxb7-GFP* transgenic mice; Wellington Cardoso and Jining Lu, for help with fluorescence stereomicroscopy; and Natalia Leach, Irfan Saadi, Kate Ackerman, Azra Ligon, David Harris, Gail Bruns, Grigoriy Kryukov, Shamil Sunyaev, Monica Banerjee, Maria Bitner-Glindzicz, Sue Malcolm, Dagan Jenkins, Ramon Bonegio, and David Salant, for helpful suggestions. This work was supported by National Institutes of Health grants PO1GM061354 (to C.C.M.) and RO1DK063316 (to R.L.M.); the Hilda Gershon Sugarman Young Investigator grant from the National Kidney Foundation, a Department of Medicine Pilot Project grant, and an Evans Medical Foundation grant (to W.L.); Dutch Kidney Foundation grant C02.2009 (to J.C.G. and A.M.v.E.); a Health Research Council grant (to M.R.E.); a Kids Kidney Appeal grant, a Kidney Research UK grant, and Wellcome Trust grant 066647 (to A.S.W. and S.A.F.); and a Medical Research Council Career Establishment grant (to W.A. and V.S.).

Appendix A

DGAP107 Phenotype

Figure A1. Facial and limb abnormalities of the DGAP107 proband. Note the low-set, dysplastic ears and subtle membranous syndactyly and clinodactyly. Blepharophimosis is also present.

Table A1. Clinical Findings in the DGAP107 Subject at Age 14 Years

Characteristic	Patient Phenotype
Weight (kg)	40 (10th percentile)
Height (cm)	146 (<5th percentile)
Visual disorders	Daltonism, strabismus, hypermetropia
Limb defects	Mild syndactyly, clinodactyly, brachymetacarpia
Urinary tract defects	VUR grade IV, bilateral UVJ defects, unilateral megaureter
Learning disabilities	Global verbal retardation, verbal IQ 69, performance IQ 46[a]
Facial features	Blepharophimosis, low-set and dysplastic ears
Dental anomalies	Malformed lower incisor ("T" shape)
Genital anomalies	Complete left testicular agenesis
Neurological defects	Seizures, hyperactivity, sleep disorder
Orthopedic abnormality	Hyperlordosis
Growth retardation	Delayed puberty
Other abnormalities	Bilateral inguinal hernia

[a] IQ = intelligence quotient.

Appendix B

The DGAP107 3p12 Breakpoint Disrupts *ROBO2*

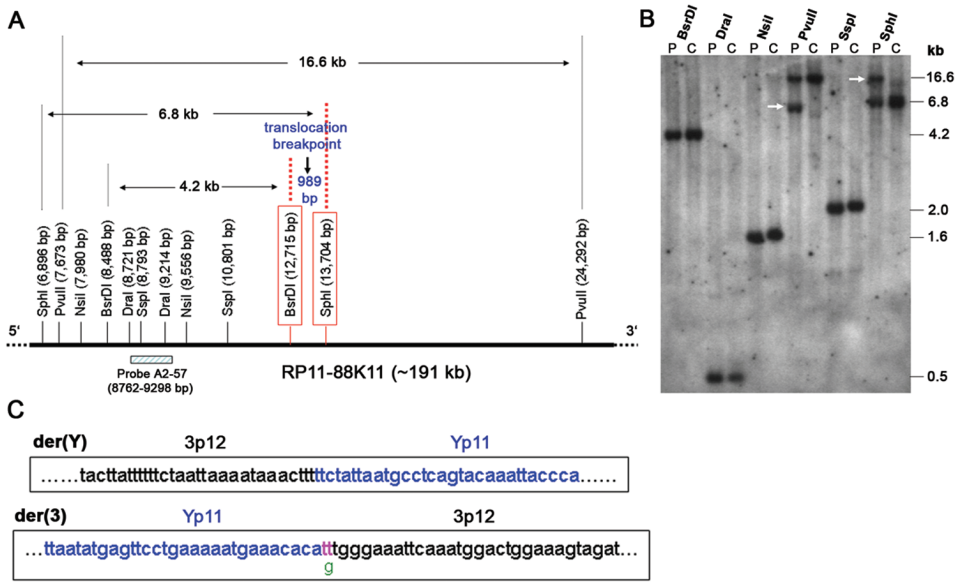

Figure B1. *ROBO2* disrupted in DGAP107, with the breakpoint lying within intron 2. *A,* Restriction map surrounding the 3p12 breakpoint. The base-pair position of BAC RP11-88K11 (AC131005, within intron 2 of *ROBO2* [see BAC contig in fig. 1*F*]) was used to calculate the distance between restriction enzyme sites. RP11-88K11 overlaps with BAC clone RP11-54A6 used in FISH and also contains the breakpoint, which is between boxed *Bsr*DI and *Sph*I sites, on the basis of the aberrant bands detected by Southern blot analysis. *B,* Southern blot analysis of DGAP107 (P) and unaffected control (C) genomic DNA, with use of the designated restriction enzymes and the probe A2-57 shown in panel A. Aberrant bands (*white arrows*) are present only in DGAP107 DNA digested with *Sph*I and *Pvu*II. *C,* Breakpoint cloning showing the sequence of the junction fragment from der(3) with a 1-bp deletion (g [*green*]) and a 2-bp insertion (tt [*pink*]). There is no gain or loss of nucleotides at the der(Y) breakpoint.

Appendix C

ROBO2 and *PCDH11Y* Expression in Human Adult and Fetal Tissues

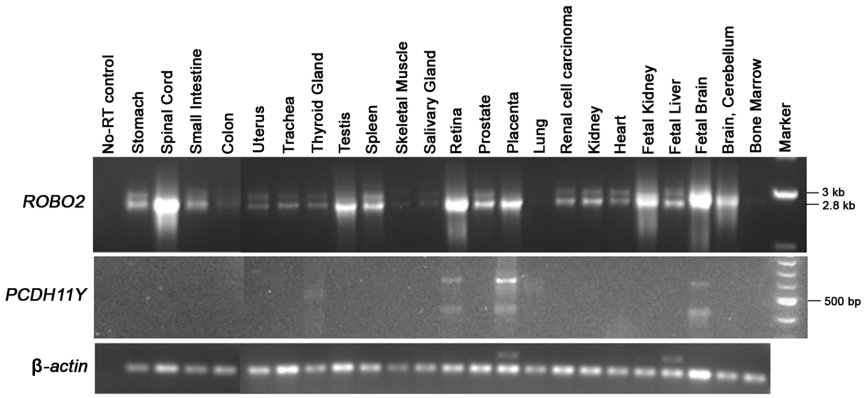

Figure C1. Expression of *ROBO2* and *PCDH11Y* in human tissues. RT-PCR amplified 2.8-kb *ROBO2* cDNAs with the use of primers *ROBO2-F1* and *ROBO2-R1*. The 3-kb *ROBO2* cDNA product (*upper band of doublet*) contains an alternatively spliced exon 24B. RT-PCR amplification of 404-bp and 620-bp *PCDH11Y* cDNAs used primers *PCDH11Y-F1* and *PCDH11Y-R1*. The intensity of the fragments indicates the approximate expression level of *ROBO2* and *PCDH11Y* in these tissues. Notably, there is no expression of *PCDH11Y* in the fetal kidney. *β-actin* was used as a cDNA loading control.

Appendix D

Analysis of the DGAP107 del(17)(p11.2) Microdeletion

The pleiotropic nature of the DGAP107 phenotype suggests that both the t(Y;3)(p11;p12)dn translocation and the del(17)(p11.2) microdeletion may contribute to the overall DGAP107 phenotype. However, we parse the contribution of del(17)(p11.2) to the VUR phenotype as follows. Point mutations in *RAI1,* which resides in the SMS critical deletion region, suggest that *RAI1* haploinsufficiency accounts for many features of SMS.[38] Less frequently observed cardiac, renal, and other defects may reflect hemizygosity for other genes in the SMS common deletion region.[39] Of note, *RAI1* is included in the 3.4-Mb del(17)(p11.2) in DGAP107, the boundaries of which were defined by FISH experiments (not shown). It seems likely that the del(17)(p11.2) microdeletion contributes to some aspects of the sleep, behavioral, and cognitive deficits in DGAP107, because similar phenotypes are observed in patients with SMS who exhibit 17p11.2 deletions or *RAI1* haploinsufficiency. Thus, *ROBO2* disruption, 17p11.2 microdeletion, or both could theoretically account for VUR in DGAP107. Our human and mouse experimental results indicate that *ROBO2* disruption can contribute substantially to the VUR phenotype. Conversely, our analyses also suggest that, whereas the 17p11.2 microdeletion in DGAP107 may contribute to the pathogenesis of VUR in DGAP107, it is not likely to play a primary role. There are three bases for this conclusion.

First, although we note an isolated case report describing VUR in SMS,[40] reexamination of the frequency of renal defects in SMS indicates that these are relatively infrequent and less frequent than originally believed.[23,41]

Second, in the context of this study, we examined and observed no kidney or collecting system defects in three age-matched genetically engineered mouse models of SMS: $SMS^{df(11)17/+}$ (Δ2 Mb), $SMS^{df(11)17-l/+}$ (Δ500 kb), and $Rai1^{-/-}$.[42–44] The first two models represent deletion alleles that eliminate 2 Mb and 500 kb, respectively, from mouse chromosome 11. These regions are homologous to and share conservation of synteny with the 17p11.2 region that is involved in SMS. Although $SMS^{df(11)17}$ and $SMS^{df(11)17-l}$ homozygotes die before nephrogenesis (9.5 embryonic d), examination of 20 $SMS^{df(11)17-l/+}$ mice in the context of this study revealed no UVJ or other urinary tract defects. In addition, $Rai1^{-/-}$ are not reported to exhibit any evidence for renal or ureteral defects,[42] and our own analysis of these mice confirms this finding.

Third, analysis of the urinary tract in five $SMS^{df(11)17-l/+}$;$Robo2^{del5/+}$ transheterozygotes, the genotype of which nominally approximates the DGAP107 genotype, revealed no observable phenotype compared with genetic background and age-matched littermate controls. Thus, whereas the 17p11.2 microdeletion could be a contributory factor, it seems unlikely to play a major role in the pathogenesis of CAKUT and VUR phenotypes in DGAP107.

Appendix E

Clinical Data for Families 2559x and B5

Clinical Data for Family 2559x

2559x is a white British family. The index patient (25592) has bilateral VUR and bilateral nephropathy. She presented at age 3 years with a symptomatic, documented *Escherichia coli* UTI, at which time ultrasound (US) revealed two small kidneys that were each 6.0 cm long (normal mean for age 7.0 cm). An indirect isotope cystogram with mercaptoacetyltriglycine (MAG3) showed bilateral VUR. The patient was treated long term with antibiotics. At age 4 years, her plasma creatinine was 107 μmol/liter (normal mean for age 56 μmol/liter). Her formal EDTA-glomerular filtration rate was 31 ml/min/1.73 m^2 (normal mean >90 ml/min/1.73 m^2), and a formal voiding cystourethrogram (VCUG) confirmed bilateral VUR. A repeat US confirmed two small kidneys with dimensions of 4.7 cm (left) and 6.0 cm (right) (50th percentile for age 7.2 cm), both with scarred upper poles. At age 9 years, she had progressive renal failure with a plasma creatinine of 306 μmol/liter. By age 12 years, her plasma creatinine had risen to 407 μmol/liter. Her mother (25593) has a history of VUR that required ureteral reimplantation surgery.

Clinical Data for Family B5

B5 is a white Dutch family. By VCUG and intravenous pyelogram (IVP), we determined that the proband B5 had bilateral VUR and a right kidney duplex system. US investigations further documented the proband's double collecting system on the right side and a single system on the left, with a slightly dilated upper pole system. Renal US studies were also performed in all other family members except grandfather B1, who is deceased. The US findings for family B5 include the following: A1 (uncle) had normal kidneys, with an 11.0-cm right kidney and a 12.5-cm left kidney (normal [$\pm$SD] 11.5 $\pm$ 1.0 cm); C1 (grandmother) had a small, 9.6-cm right kidney, an 11.4-cm left kidney, a slim collecting system on both sides, a normal corticomedullary ratio, no signs of a duplex system, and normal flow in the right renal artery; D1 (aunt) had an 11.8-cm right kidney with an upper pole duplex system (column of Bertini), an 11.0-cm left kidney, a normal corticomedullary ratio, and no dilatation or urologic complaints; E1 (father) had a normal kidneys, a slim collecting system on both sides, a small peripelvic cyst on the right side, and no urologic complaints; F1 (mother) had a left kidney with fetal lobulation on the right side, no visible column from the renal parenchyma to the hilus, a duplex system that can neither be proven nor excluded, a slim collecting system on both sides, and febrile UTI history; and G1 (aunt) had no dilatation on either kidney, a cyst (4.8 × 3.5 cm) in the upper pole of the left kidney, and pyelonephritis at age 8 years.

Controls

All controls for genetic studies of families 2559x and B5 were unrelated. Control samples were from 180 Americans of white European descent (CEPH) and from 96 whites in the same geographic region as family B5. These latter 96 samples were subjected both to targeted sequencing of exons 12, 19, and 23 and to complete resequencing of all 26 coding *ROBO2* exons.

Appendix F

Analysis of *Robo*^{del5} Mutant Mice

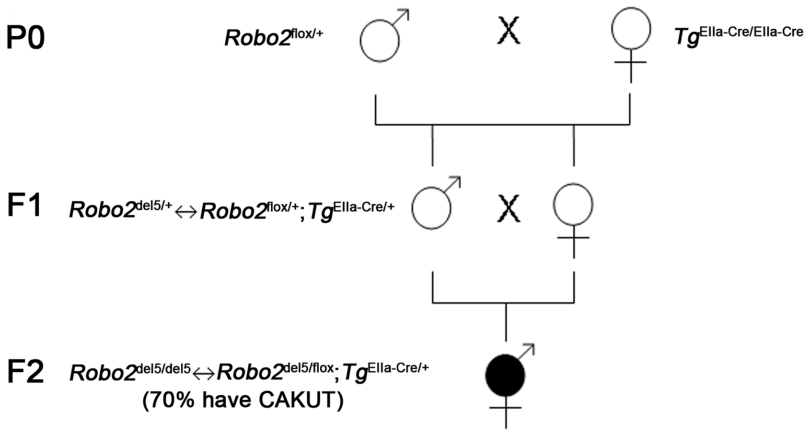

Figure F1. Generation of F2 *Robo2*$^{del5/del5}$↔*Robo2*$^{del5/flox}$ mosaics

Table F1. Phenotype-Genotype Correlation in F2 *Robo2*$^{del5/del5}$↔*Robo2*$^{del5/flox}$ Mosaics

Identification Number	Age (d)	Sex	Phenotype[a]
3235	45	F	L and R: megaureter, hydronephrosis
3239	45	F	R: megaureter, hydronephrosis; L: normal
404	62	M	L: megaureter, hydronephrosis with complete loss of renal parenchyma; R: normal
3218	77	M	R: megaureter, hydronephrosis with complete loss of renal parenchyma; L: normal
3236	77	F	No discernible gross phenotype
403	62	M	No discernible gross phenotype
3372	27	M	No discernible gross phenotype
3964	20	F	L: megaureter, hydronephrosis; R: normal
3963	20	F	L: megaureter, hydronephrosis; R: normal
3962	20	F	L and R: megaureter, hydronephrosis

NOTE.—Genotyping was performed using PCR of mouse tail DNA. All mosaics were positive for *Robo2*^{del5}, *Robo2*^{flox}, and Tg$^{EIIa\text{-}Cre}$.

[a] L = left; R = right.

Notes on the Breeding Scheme

In the P0 generation, *Robo2*$^{flox/+}$ heterozygotes were crossed with *Tg*$^{EIIa\text{-}cre/EIIa\text{-}cre}$ homozygotes. The 50% of the progeny that receive *Tg*$^{EIIa\text{-}cre}$ and *Robo2*^{flox} gametes constitute the F1 generation shown (fig. F1). When transmitted from males, *Tg*$^{EIIa\text{-}cre}$ is variably expressed in the F1 embryos after fertilization and before implantation,[29,31] resulting in recombination in some embryonic cells but not others. Thus, the resulting F1 progeny are mosaic and contain mixtures of *Robo2*$^{flox/+}$ (no recombination) and *Robo2*$^{del5/+}$ (recombination) cells. These mosaics are genotypically denoted *Robo2*$^{del5/+}$↔*Robo2*$^{flox/+}$;*Tg*$^{EIIa\text{-}cre/+}$. PCR experiments demonstrated variable ratios of the *Robo2*^{flox} and the *Robo2*^{del5} alleles, confirming the mosaicism of the F1 mice (not shown). As expected, 10 F1 mosaic mice examined exhibit no observable phenotype, because heterozygous *Robo2*$^{del5/+}$ mice exhibit a phenotype at a low percentage (i.e., 15%), and, even at the most extreme degree of mosaicism (100% *Robo2*$^{del5/+}$ and 0% *Robo2*$^{flox/+}$), the overall reduction in *Robo2* gene dosage would not surpass that in *Robo2*$^{del5/+}$ heterozygotes.

The F2 generation was generated by intercross of the subset of F1 germline mosaics that also carried the *Tg*$^{E11a\text{-}cre/+}$ transgene. The F2 generation thus also consisted of mosaic progeny because of the union of *Robo2*^{del5};*Tg*$^{EIIa\text{-}cre}$ and *Robo2*^{flox} gametes. This particular combination of gametes results in a subset of F2 mosaics that contains both *Robo2*$^{del5/del5}$ and *Robo2*$^{del5/flox}$ cells—that is, a mixture of heterozygous and homozygous cells. Cells carrying the *Robo2*$^{del5/del5}$ genotype in these *Robo2*$^{del5/del5}$↔*Robo2*$^{del5/flox}$ mosaics derive from the action of Cre in cells that commence embryogenesis with the *Robo2*$^{del5/flox}$ genotype; *Robo2*$^{del5/flox}$ cells result when Cre activity in those cells is insufficient to cause recombination. As described in the text and in table F1, 70% of these mosaics exhibit striking CAKUT phenotypes, whereas 30% exhibit no observable phenotype. The presence of a CAKUT phenotype presumably correlates with the percentage of *Robo2*$^{del5/del5}$ cells that make up the urinary tracts of these mosaics.

The mosaic nature of the F2 mice (at least in the germline) was established by further intercross of a subset of F2 *Robo2*$^{del5/del5}$↔*Robo2*$^{del5/flox}$;*Tg*$^{EIIa\text{-}cre}$ mosaics to generate an F3 generation. In this case, a high percentage of *Robo2*$^{del5/del5}$ cells in the F2 germline result in a preponderance of gametes carrying the *Robo2*^{del5} mutant allele. The union of these *Robo2*^{del5} gametes results in an increased proportion of *Robo2*$^{del5/del5}$ mice (90% of progeny) in the F3 generation that die at birth from CAKUT phenotypes (not shown). The remaining 10% retain the *Robo2*$^{del5/flox}$ allele and survive. The non-Mendelian ratio of these resulting F3 genotypes confirms germline mosaicism in the F2 mice.

Appendix G

PCR Primers

Table G1. PCR Primers and Probes

Primer or Probe Used[a]	Type	Location	Sequence
RT-PCR analyses:			
2.8-kb *ROBO2* cDNA[b]:			
ROBO2-F1	Forward	Exon 9 of *ROBO2*	5′-GAGCAAGGCACACTGCAGATTA-3′
ROBO2-R1	Reverse	Exon 26 of *ROBO2*	5′-AGTCATCACTTCCATGAGTCCG-3′
404-bp and 620-bp *PCDH11Y* cDNA[b]:			
PCDH11Y-F1	Forward	Exon 1 of *PCDH11Y*	5′-CAGAAACAACCTCAGCGACTCC-3′
PCDH11Y-R1	Reverse	Exon 4 of *PCDH11Y*	5′-GAACACCACGCATACTAGCAGG-3′
ROBO2-PCDH11Y fusion transcripts[c]:			
ROBO2-F2	Forward	Exon 2 of *ROBO2*	5′-GCAGTGAGTCGAAATGCGTC-3′
PCDH11Y-R1	Reverse	Exon 4 of *PCDH11Y*	5′-GAACACCACGCATACTAGCAGG-3′
PCDH11Y-R2	Reverse	Exon 3 of *PCDH11Y*	5′-CCCACTGTCATTCAGTCCTCAT-3′
PCDH11Y-R3	Reverse	Exon 5 of *PCDH11Y*	5′-TGTTTCAATGACATCGAGGCC-3′
606-bp *ROBO2* nontranslocated allele[c]:			
ROBO2-F2	Forward	Exon 2 of *ROBO2*	5′-GCAGTGAGTCGAAATGCGTC-3′
ROBO2-qR	Reverse	Exon 7 of *ROBO2*	5′-TGGCCGAACCACAAACTGT-3′
Quantitative real-time PCR analyses:			
ROBO2 nontranslocated allele[d]:			
ROBO2-F2	Forward	Exon 2 of *ROBO2*	5′-GCAGTGAGTCGAAATGCGTC-3′
ROBO2-qR2	Reverse	Exon 3 of *ROBO2*	5′-GCTCTCCAGCTGCCACTACAA-3′
ROBO2-FAM2	TaqMan probe	*ROBO2* exon 2–exon 3 junction	5′-CTGGAAGTGGCATTGTTACGAGATGACTTCC-3′
Fu-129 transcript[d,e]:			
ROBO2-F2	Forward	Exon 2 of *ROBO2*	5′-GCAGTGAGTCGAAATGCGTC-3′
PCDH11Y-qR1	Reverse	Exon 1d of *PCDH11Y*	5′-TATTCCATCCTCTTCCATCCATTC-3′
TaqMan 129	TaqMan probe	*ROBO2* exon 2 and *PCDH11Y* exon 1d junction	5′-CTGGAAGTGGCATAGGGTGCTTAAAAAGTACAGA-3′
Fu-153 transcript[d,e]:			
ROBO2-F2	Forward	Exon 2 of *ROBO2*	5′-GCAGTGAGTCGAAATGCGTC-3′
PCDH11Y-qR2	Reverse	Exon 4 of *PCDH11Y*	5′-ATGTACGTCCCGGACAACAAA-3′
TaqMan 153	TaqMan probe	*ROBO2* exon 2 and *PCDH11Y* exon 4 junction	5′-TGGAAGTGGCATTGTTGTGCGGGT-3′
Genotyping of *Robo2*^{flox} and *Robo2*^{del5} mice:			
Robo2^{flox} allele[f]:			
Ro2-MEBAC15F	Forward	Intron 5 of *Robo2*	5′-CCAATCATAGTCTCTCCACG-3′
Ro2-MEBAC15R	Reverse	Intron 5 of *Robo2*	5′-CCTCTGATTCAATGAGATGC-3′
1,180-bp fragment from *Robo2*^{del5} allele:			
Robo2koF	Forward	Intron 4 of *Robo2*	5′-CCACTATGCTGGCTCTGTCTCACAC-3′
Robo2R	Reverse	Intron 5 of *Robo2*	5′-GGTTTTGGAGGTCTTACTACGTAGC-3′
1,390-bp fragment from *Robo2*$^{+}$ wild-type allele:			
Robo2wtF	Forward	Intron 4 of *Robo2*	5′-CAACTTTTCCTTTTCCGGGAGG-3′
Robo2R	Reverse	Intron 5 of *Robo2*	5′-GGTTTTGGAGGTCTTACTACGTAGC-3′
Synthesis of fusion protein constructs:			
Fu-129 *ROBO2-PCDH11Y* fusion cDNA (129-aa fusion protein):			
5′-hR2(E1)	Forward	Exon 1 of *ROBO2* with 5′ *EcoRI* linker	5′-ATCGAATTCATGAGTCTGCTGATGTTTACACAAC-TACTG-3′
3′-LEVA(X1)	Reverse	Intron 1d of *PCDH11Y* with 5′ *XhoI* linker	5′-TTACTCGAGCTATGCCACTTCCAGAGACGCATTTCG-3′
Fu-153 *ROBO2-PCDH11Y* fusion cDNA (153-aa fusion protein):			
5′-hR2(E1)	Forward	Exon 1 of *ROBO2* with 5′ *EcoRI* linker	5′-ATCGAATTCATGAGTCTGCTGATGTTTACACAAC-TACTG-3′
3′-SRSC(X1)	Reverse	Intron 4 of *PCDH11Y* with 5′ *XhoI* linker	5′-CCACTCGAGCTAGCAGGACCGCGAAAATGTACGTCC-3′

[a] Primers and probes were used for amplification and quantitation.

[b] As shown in figure C1.

[c] As shown in figure 2*B*.

[d] As shown in figure 2*C*.

[e] As shown in figure 2*D*.

[f] PCR amplifies a 1,100-bp fragment from both wild-type and *Robo2*^{flox} alleles. After *Spe*I digestion, *Robo2*^{flox} allele will not cleave (1,100-bp product), whereas the wild-type allele will be cleaved by *Spe*I to yield two smaller products of 750 bp and 350 bp.

Table G2. PCR Primer Sets Used to Amplify 26 Human *ROBO2* Exons and Intron-Exon Boundaries in Mutation Analysis

Exon and Primer	Amplicon Size (bp)	Location in *ROBO2*	Sequence
1:	286		
Forward		5′-UTR	5′-TTTGCTCTTCTTGACTTTAATTAGTATCTAGG-3′
Reverse		Introns 1–2	5′-TATAACCCACATCAAATTCAAAAAGAAAT-3′
2:	501		
Forward		Introns 1–2	5′-CGAAGAGTTTAATTTCCCCATCA-3′
Reverse		Introns 2–3	5′-GCGTCTATGGGAACACATCAAAA-3′
3:	264		
Forward		Introns 2–3	5′-TTGTACAACAAAAAGCCTAAGTTACTGTC-3′
Reverse		Introns 3–4	5′-AAAATTCAATCTCTCTGGGCCAT-3′
4:	280		
Forward		Introns 3–4	5′-TAATGACCTTTATTTTCTATTCTGTTCCTTT-3′
Reverse		Introns 4–5	5′-TTATATGGCCCAGTTTTTAATGTTAGTAATACT-3′
5:	291		
Forward		Introns 4–5	5′-CTTTTTTCATAATGTACTTAAAGCATGCA-3′
Reverse		Introns 5–6	5′-GTGGCATTGTAGCTGTCCTTTTATT-3′
6:	427		
Forward		Introns 5–6	5′-TTGCACTTTGTGGCTGATTTG-3′
Reverse		Introns 6–7	5′-TAATTTTATTTCAACTAATGATAGAGAGGACAC-3′
7:	289		
Forward		Introns 6–7	5′-CAACATAGTACCATATTTTCTCCTTGACATA-3′
Reverse		Introns 7–8	5′-AAGCAAGGCAAGCTTTCAGG-3′
8:	336		
Forward		Introns 7–8	5′-CCCACTGTATTCCTTAATTGTAGTAGCTT-3′
Reverse		Introns 8–9	5′-TCCACATGGTTAACGTGTATCTAGAAA-3′
9:	351		
Forward		Introns 8–9	5′-TTCAGTGTCAATATATCAAGCCTACTGA-3′
Reverse		Introns 9–10	5′-CACTATGCAATTTTTCCATAGAGCAG-3′
10:	231		
Forward		Introns 9–10	5′-TGGCTGTCATTGAGTAATTATTCTGC-3′
Reverse		Introns 10–11	5′-TCCCCCCTTAACTTATTATTTGATATTG-3′
11:	343		
Forward		Introns 10–11	5′-CTGTCTAGGTCAGGTCCTTTAGTAGACTG-3′
Reverse		Introns 11–12	5′-CAGCAGGATAGTTCAGGTGACATT-3′
12:	324		
Forward		Introns 11–12	5′-AACCTTTGTCATTGATACCCAACTC-3′
Reverse		Introns 12–13	5′-TCCTCATCAAGCCCCTCGT-3′
13:	298		
Forward		Introns 12–13	5′-AGTTCTAAAGACATGAGGTTGATTTACATAA-3′
Reverse		Introns 13–14	5′-CACTCTTTGTTCATTTGCATTTTCC-3′
14:	409		
Forward		Intron 13–14	5′-AGGACAGAAATGGGACAAATGAA-3′
Reverse		Intron 14–15	5′-TTCTAAGGAAGATAACAAATAGGTACTGTAACA-3′
15:	294		
Forward		Introns 14–15	5′-AGTCTCCTGCAACTTGTCTTTATACTCAT-3′
Reverse		Introns 15–16	5′-TCATTCGTGAGACACTGAGATTTCT-3′
16:	321		
Forward		Introns 15–16	5′-AATATTTGATCAGTTACAGTAGTCTCGTTACC-3′
Reverse		Introns 16–17	5′-TGCAAAATCATCATCCACCTTG-3′
17:	338		
Forward		Introns 16–17	5′-TCTTCATTTTTGATGCACCATGT-3′
Reverse		Introns 17–18	5′-TTTCTGTTCCTTCCATTCATTTCAT-3′
18:	211		
Forward		Introns 17–18	5′-CCTCAGCTCTAAACTAAGGGCCA-3′
Reverse		Introns 18–19	5′-TCTTACTATAGAGTTTCCCCAGTCCTG-3′
19:	240		
Forward		Introns 18–19	5′-AAATCTTCCATTTCTTAACGCTTTATATTG-3′
Reverse		Introns 19–20	5′-AAAAACACAACTTACCTCCACGG-3′
20:	432		

(*continued*)

Table G2. (continued)

Exon and Primer	Amplicon Size (bp)	Location in *ROBO2*	Sequence
Forward		Introns 19–20	5′-GATAGTTTTGGGCTTCCGGTG-3′
Reverse		Introns 20–21	5′-TGAATCACTAAGTCAAACAACAAATACTAATT-3′
21:	306		
Forward		Introns 20–21	5′-CATAAATACACCTTGCCATCTGATG-3′
Reverse		Introns 21–22	5′-TGGCAAAAATGAACAACAGAGAG-3′
22:	411		
Forward		Introns 21–22	5′-TGCATGTATGTGTATATGTATTTGTGTCA-3′
Reverse		Introns 22–23	5′-TGTAGTTCTATCAGAATCTCTTGTGAATTTATT-3′
23:	379		
Forward		Introns 22–23	5′-AAGACAGTATGAGTTACTATAGCATGCATTT-3′
Reverse		Introns 23–24	5′-GGAAGTAGTTGACTTTTGATGCATTTTA-3′
24:	325		
Forward		Introns 23–24	5′-AGGTAGATTTACAGGTTAGTCATAGTGCA-3′
Reverse		Introns 24–25	5′-CATGGAGCACGTCTCTTCAGC-3′
25:	351		
Forward		Introns 24–25	5′-TGGTAAAGTAGGCCATTCACAGTG-3′
Reverse		Introns 25–26	5′-CAAGATTCTTTCTGAATCACGATAGC-3′
26:	574		
Forward		Introns 25–26	5′-TCACAAACTCATCTATCTGAAGACCTTAT-3′
Reverse		3′-UTR	5′-AAAATTGCAGTGCAAAATTTAAACA-3′

Web Resources

Accession numbers and URLs for data presented herein are as follows:

BACPAC Resources, http://bacpac.chori.org/
DGAP, http://dgap.harvard.edu/
Ensembl, http://www.ensembl.org/Homo_sapiens/index.html
Entrez Protein, http://www.ncbi.nlm.nih.gov/entrez/query.fcgi?db=Protein (for ROBO2 [accession number NP_002933])
GenBank, http://www.ncbi.nlm.nih.gov/Genbank/ (for *ROBO2* [accession number NM_002942] and *PCDH11Y* [accession number NM_032971])
Online Mendelian Inheritance in Man (OMIM), http://www.ncbi.nlm.nih.gov/Omim/ (for VUR and SMS)

References

1. Pope JC 4th, Brock JW 3rd, Adams MC, Stephens FD, Ichikawa I (1999) How they begin and how they end: classic and new theories for the development and deterioration of congenital anomalies of the kidney and urinary tract, CAKUT. J Am Soc Nephrol 10:2018–2028
2. Nakanishi K, Yoshikawa N (2003) Genetic disorders of human congenital anomalies of the kidney and urinary tract (CAKUT). Pediatr Int 45:610–616
3. Feather SA, Malcolm S, Woolf AS, Wright V, Blaydon D, Reid CJ, Flinter FA, Proesmans W, Devriendt K, Carter J, et al (2000) Primary, nonsyndromic vesicoureteric reflux and its nephropathy is genetically heterogeneous, with a locus on chromosome 1. Am J Hum Genet 66:1420–1425
4. Sargent MA (2000) What is the normal prevalence of vesicoureteral reflux? Pediatr Radiol 30:587–593
5. Bailey RR (1973) The relationship of vesico-ureteric reflux to urinary tract infection and chronic pyelonephritis-reflux nephropathy. Clin Nephrol 1:132–141
6. Dillon MJ, Goonasekera CD (1998) Reflux nephropathy. J Am Soc Nephrol 9:2377–2383
7. Kincaid-Smith PS, Bastos MG, Becker GJ (1984) Reflux nephropathy in the adult. Contrib Nephrol 39:94–101
8. Mackie GG, Awang H, Stephens FD (1975) The ureteric orifice: the embryologic key to radiologic status of duplex kidneys. J Pediatr Surg 10:473–481
9. Noe HN, Wyatt RJ, Peeden JN Jr, Rivas ML (1992) The transmission of vesicoureteral reflux from parent to child. J Urol 148:1869–1871
10. Van den Abbeele AD, Treves ST, Lebowitz RL, Bauer S, Davis RT, Retik A, Colodny A (1987) Vesicoureteral reflux in asymptomatic siblings of patients with known reflux: radionuclide cystography. Pediatrics 79:147–153
11. Kidd T, Brose K, Mitchell KJ, Fetter RD, Tessier-Lavigne M, Goodman CS, Tear G (1998) Roundabout controls axon crossing of the CNS midline and defines a novel subfamily of evolutionarily conserved guidance receptors. Cell 92:205–215
12. Xian J, Aitchison A, Bobrow L, Corbett G, Pannell R, Rabbitts T, Rabbitts P (2004) Targeted disruption of the 3p12 gene, Dutt1/Robo1, predisposes mice to lung adenocarcinomas and lymphomas with methylation of the gene promoter. Cancer Res 64:6432–6437
13. Xian J, Clark KJ, Fordham R, Pannell R, Rabbitts TH, Rabbitts PH (2001) Inadequate lung development and bronchial hyperplasia in mice with a targeted deletion in the *Dutt1/Robo1* gene. Proc Natl Acad Sci USA 98:15062–15066
14. Hannula-Jouppi K, Kaminen-Ahola N, Taipale M, Eklund R, Nopola-Hemmi J, Kaariainen H, Kere J (2005) The axon guidance receptor gene *ROBO1* is a candidate gene for developmental dyslexia. PLoS Genet 1:e50
15. Jen JC, Chan WM, Bosley TM, Wan J, Carr JR, Rub U, Shattuck D, Salamon G, Kudo LC, Ou J, et al (2004) Mutations in a human *ROBO* gene disrupt hindbrain axon pathway crossing and morphogenesis. Science 304:1509–1513
16. Bedell VM, Yeo SY, Park KW, Chung J, Seth P, Shivalingappa V, Zhao J, Obara T, Sukhatme VP, Drummond IA, et al (2005) *Roundabout4* is essential for angiogenesis in vivo. Proc Natl Acad Sci U S A 102:6373–6378

17. Fricke C, Lee JS, Geiger-Rudolph S, Bonhoeffer F, Chien CB (2001) *Astray,* a zebrafish roundabout homolog required for retinal axon guidance. Science 292:507–510
18. Long H, Sabatier C, Ma L, Plump A, Yuan W, Ornitz DM, Tamada A, Murakami F, Goodman CS, Tessier-Lavigne M (2004) Conserved roles for Slit and Robo proteins in midline commissural axon guidance. Neuron 42:213–223
19. Grieshammer U, Le M, Plump AS, Wang F, Tessier-Lavigne M, Martin GR (2004) SLIT2-mediated ROBO2 signaling restricts kidney induction to a single site. Dev Cell 6:709–717
20. Li HS, Chen JH, Wu W, Fagaly T, Zhou L, Yuan W, Dupuis S, Jiang ZH, Nash W, Gick C, et al (1999) Vertebrate slit, a secreted ligand for the transmembrane protein roundabout, is a repellent for olfactory bulb axons. Cell 96:807–818
21. Ward ME, Rao Y (2005) Investigations of neuronal migration in the central nervous system. Methods Mol Biol 294:137–156
22. Blanco P, Sargent CA, Boucher CA, Mitchell M, Affara NA (2000) Conservation of PCDHX in mammals; expression of human X/Y genes predominantly in brain. Mamm Genome 11:906–914
23. Potocki L, Shaw CJ, Stankiewicz P, Lupski JR (2003) Variability in clinical phenotype despite common chromosomal deletion in Smith-Magenis syndrome [del(17)(p11.2p11.2)]. Genet Med 5:430–434
24. Liu Z, Patel K, Schmidt H, Andrews W, Pini A, Sundaresan V (2004) Extracellular Ig domains 1 and 2 of Robo are important for ligand (Slit) binding. Mol Cell Neurosci 26:232–240
25. Wu W, Wong K, Chen J, Jiang Z, Dupuis S, Wu JY, Rao Y (1999) Directional guidance of neuronal migration in the olfactory system by the protein Slit. Nature 400:331–336
26. Chapman CJ, Bailey RR, Janus ED, Abbott GD, Lynn KL (1985) Vesicoureteric reflux: segregation analysis. Am J Med Genet 20:577–584
27. Li X, Chen Y, Liu Y, Gao J, Gao F, Bartlam M, Wu JY, Rao Z (2006) Structural basis of Robo proline-rich motif recognition by the srGAP1 Src homology 3 domain in the Slit-Robo signaling pathway. J Biol Chem 281:28430–28437
28. Wong K, Ren XR, Huang YZ, Xie Y, Liu G, Saito H, Tang H, Wen L, Brady-Kalnay SM, Mei L, et al (2001) Signal transduction in neuronal migration: roles of GTPase activating proteins and the small GTPase Cdc42 in the Slit-Robo pathway. Cell 107:209–221
29. Lakso M, Pichel JG, Gorman JR, Sauer B, Okamoto Y, Lee E, Alt FW, Westphal H (1996) Efficient in vivo manipulation of mouse genomic sequences at the zygote stage. Proc Natl Acad Sci USA 93:5860–5865
30. Srinivas S, Goldberg MR, Watanabe T, D'Agati V, al-Awqati Q, Costantini F (1999) Expression of green fluorescent protein in the ureteric bud of transgenic mice: a new tool for the analysis of ureteric bud morphogenesis. Dev Genet 24:241–251
31. Holzenberger M, Lenzner C, Leneuve P, Zaoui R, Hamard G, Vaulont S, Bouc YL (2000) Cre-mediated germline mosaicism: a method allowing rapid generation of several alleles of a target gene. Nucleic Acids Res 28:E92
32. Tanagho EA, Guthrie TH, Lyon RP (1969) The intravesical ureter in primary reflux. J Urol 101:824–832
33. Stauss J, Connolly LP, Connolly SA, Zurakowski D, Treves ST, Peters CA (2003) Dynamic renal scintigraphy in children with vesicoureteral reflux and suspected coexisting ureteropelvic junction obstruction. J Urol 170:1966–1970
34. Batourina E, Tsai S, Lambert S, Sprenkle P, Viana R, Dutta S, Hensle T, Wang F, Niederreither K, McMahon AP, et al (2005) Apoptosis induced by vitamin A signaling is crucial for connecting the ureters to the bladder. Nat Genet 37:1082–1089
35. Sanna-Cherchi S, Reese A, Hensle T, Caridi G, Izzi C, Kim YY, Konka A, Murer L, Scolari F, Ravazzolo R, et al (2005) Familial vesicoureteral reflux: testing replication of linkage in seven new multigenerational kindreds. J Am Soc Nephrol 16:1781–1787
36. Eccles MR, Bailey RR, Abbott GD, Sullivan MJ (1996) Unravelling the genetics of vesicoureteric reflux: a common familial disorder. Hum Mol Genet 5:1425–1429
37. Yue Y, Grossmann B, Galetzka D, Zechner U, Haaf T (2006) Isolation and differential expression of two isoforms of the *ROBO2/Robo2* axon guidance receptor gene in humans and mice. Genomics 88:772–778
38. Slager RE, Newton TL, Vlangos CN, Finucane B, Elsea SH (2003) Mutations in RAI1 associated with Smith-Magenis syndrome. Nat Genet 33:466–468
39. Bi W, Yan J, Stankiewicz P, Park SS, Walz K, Boerkoel CF, Potocki L, Shaffer LG, Devriendt K, Nowaczyk MJ, et al (2002) Genes in a refined Smith-Magenis syndrome critical deletion interval on chromosome 17p11.2 and the syntenic region of the mouse. Genome Res 12:713–728
40. Chou IC, Tsai FJ, Yu MT, Tsai CH (2002) Smith-Magenis syndrome with bilateral vesicoureteral reflux: a case report. J Formos Med Assoc 101:726–728
41. Greenberg F, Lewis RA, Potocki L, Glaze D, Parke J, Killian J, Murphy MA, Williamson D, Brown F, Dutton R, et al (1996) Multi-disciplinary clinical study of Smith-Magenis syndrome (deletion 17p11.2). Am J Med Genet 62:247–254
42. Bi W, Ohyama T, Nakamura H, Yan J, Visvanathan J, Justice MJ, Lupski JR (2005) Inactivation of *Rai1* in mice recapitulates phenotypes observed in chromosome engineered mouse models for Smith-Magenis syndrome. Hum Mol Genet 14: 983–995
43. Walz K, Caratini-Rivera S, Bi W, Fonseca P, Mansouri DL, Lynch J, Vogel H, Noebels JL, Bradley A, Lupski JR (2003) Modeling del(17)(p11.2p11.2) and dup(17)(p11.2p11.2) contiguous gene syndromes by chromosome engineering in mice: phenotypic consequences of gene dosage imbalance. Mol Cell Biol 23:3646–3655
44. Yan J, Keener VW, Bi W, Walz K, Bradley A, Justice MJ, Lupski JR (2004) Reduced penetrance of craniofacial anomalies as a function of deletion size and genetic background in a chromosome engineered partial mouse model for Smith-Magenis syndrome. Hum Mol Genet 13:2613–2624